JOURNAL OF SOLID STATE CHEMISTRY 114, 174–183 (1995)

Structural and Electronic Properties of the Mixed Co/Ru Perovskites $AA'CoRuO_6$ (A, A' = Sr, Ba, La)

S. H. Kim and P. D. Battle*

Inorganic Chemistry Laboratory, South Parks Road, Oxford, OX1 3QR, United Kingdom

Received December 28, 1993; in revised form May 11, 1994; accepted May 13, 1994

The compounds Sr_2CoRuO_6, $SrLaCoRuO_6$, Ba_2CoRuO_6, and $BaLaCoRuO_6$ have been prepared and characterized by X ray powder diffraction and SQUID magnetometry. All but Ba_2CoRuO_6 crystallize as pseudo-cubic perovskites with a disordered arrangement of Co and Ru cations over the six-coordinate sites. Ba_2CoRuO_6 adopts the hexagonal 6H perovskite structure with Co in the vertex-sharing octahedra and a random arrangement of Co and Ru in the M_2O_9 dimers. Frustration is apparent in the magnetic properties of each of these compounds at low temperatures, in contrast to the 6H perovskite $Ba_3CoRu_2O_9$, which shows no structural disorder and orders antiferromagnetically at 106 K.

INTRODUCTION

The structural and electronic properties of perovskite-related materials having the general formulae $A_2BRu^{5+}O_6$ and $AA'BRu^{5+}O_6$ (where A and A' are early lanthanides or alkaline-earth metals and B is a transition metal or one of the smaller lanthanides) have been extensively investigated by a number of research groups, including ourselves (1–3). The compounds that belong to this family have a wide variety of interesting magnetic properties. If the cations B and Ru^{5+} are ordered over the six-coordinate sites of the perovskite structure, long-range magnetic order is usually observed at low temperatures with the details of the magnetic structure being dependent on the nature of the superexchange interactions involved. For example, Sr_2ErRuO_6 has an ordered 1 : 1 arrangement of Er^{3+} and Ru^{5+} over the six-coordinate sites and orders as a weak ferromagnet at ~40 K (4), whereas Sr_2YRuO_6, with a similar ordering of Ru^{5+} and diamagnetic Y^{3+}, exhibits antiferromagnetism below ~26 K (1). Unusual magnetic properties are observed when B is magnetic but the distribution of B and Ru^{5+} over the six-coordinate sites is random rather than ordered. Despite having a high concentration of magnetic cations in a nonfrustrated crystal structure, $BaLaNiRuO_6$ and Sr_2FeRuO_6 do not transform to a magnetically ordered state, but they do show a spin-glass transition (3). This surprising behavior has been explained in terms of the frustration caused by competing superexchange interactions among the random distribution of Ni/Ru and Fe/Ru cations. Similar properties have been observed in a series of compounds $Sr_nLaCuRuO_{n+5}$ (n = 1, 2, 3) and Sr_nFeRuO_{n+4} (n = 3, 4) (5, 6).

In order to investigate further the behavior of perovskite systems containing Ru^{5+} and a second paramagnetic species we have now prepared and studied A_2CoRuO_6 and $ALaCoRuO_6$ (A = Sr, Ba). $BaLaCoRuO_6$ has been prepared previously (2) and, on the basis of X ray powder diffraction patterns, it was described as a cubic perovskite with an ordered arrangement of Co^{2+} and Ru^{5+} cations. The oxidation states of Co and Ru were established by Mössbauer spectroscopy, and the susceptibility maximum observed at ~40 K was interpreted as the onset of long-range antiferromagnetic order, although the Weiss constant was found to be positive. In this paper we describe the characterization of the title compounds by X ray powder diffraction, electrical resistivity, and magnetic susceptibility measurements, and we then go on to discuss our results in terms of the magnetic frustration present in the crystal structures. Magnetic measurements on the 6H-perovskite $Ba_3Co_2RuO_9$ are also described in order to show the effect of the Co/Ru ratio and the crystal structure on the magnetic properties. The details of the low-temperature crystal and magnetic structures of this material have been published elsewhere (7).

EXPERIMENTAL

Polycrystalline samples of the title compounds were prepared by firing the appropriate quantities of $SrCO_3$, $BaCO_3$, Co_3O_4, and dried RuO_2 and La_2O_3 (all from Johnson Matthey Chemicals) in air at the temperatures listed in Table 1 for a period of several days with regular grinding and repelleting. The progress of the reactions was monitored by X ray powder diffraction, and they were deemed to be complete when accordant powder patterns

* To whom correspondence should be addressed.

0022-4596/95 $6.00

TABLE 1
Reaction Temperatures Used in the Preparation of $AA'BRuO_6$

Compound	Reaction temperature (°C)
Sr_2CoRuO_6	1200
Ba_2CoRuO_6	1150
$SrLaCoRuO_6$	1150
$BaLaCoRuO_6$	1200

were obtained. The final diffraction data were recorded at room temperature by step scanning over the angular range $15° \leq 2\theta \leq 115°$ (100° for Ba_2CoRuO_6), using a Philips automated PW 1710 diffractometer operating with CuKα radiation. A 2θ step size of 0.02° and a counting time of 10 sec per point were used. Neutron powder diffraction data were collected on $BaLaCoRuO_6$ at room temperature (λ = 1.9127 Å) and 1.5 K (λ = 1.9110 Å) using the diffractometer D1a at ILL Grenoble. The angular range $0 \leq 2\theta \leq 156°$ was scanned with a step interval of 0.05° using a 10 g sample contained in a thin-walled vanadium can. Electrical conductivity measurements were made for all the title compounds between 77 and 300 K using a standard D.C. four-probe apparatus mounted in an Oxford Instruments CF 200 cryostat. Colloidal silver paint was used to make contacts on samples of dimensions *ca.* 2 × 2 × 10 mm which had been cut from sintered pellets. The separation of the two inner (voltage) contacts was approximately 3 mm. D.C. magnetic susceptibility data were recorded in the temperature range $6 \leq T \leq 296$ K using a Cryogenic S600C SQUID magnetometer. The samples were in the form of *ca.* 100 mg of finely ground powder, packed into a quartz tube. The measurements were made in a liquid ^{4}He cryostat both after cooling the sample in zero field (ZFC) and after cooling in measuring fields of 1 and 5 kG (FC). In the case of $SrLaCoRuO_6$, an applied field of 1 kG only was used. The temperature was controlled with a Lake Shore DRC-91C regulator using a gallium–aluminium–arsenide diode sensor. The magnetic susceptibility of a previously prepared (7) sample of $Ba_3CoRu_2O_9$ was measured in a field of 1 kG over the same temperature range. The molar magnetic susceptibilities presented in this paper have been corrected for the diamagnetic contributions of the constituent atoms.

RESULTS

(i) Structural Characterization

All the X ray powder diffraction profiles collected in this study were analyzed by the Rietveld profile analysis technique (8) using version 5.1 of the GSAS software package (9). The peak shape function was assumed to be of a pseudo-Voigt type (10) and the background levels were fitted by a cosine Fourier series function using nine refinable coefficients (9). Regions of the profile containing contributions from the aluminium sample plate were excluded from the refinements. Except where otherwise stated, the oxygen sublattice was assumed to be fully occupied.

(a) A_2CoRuO_6 (A = Sr, Ba). The room temperature X ray diffraction data from Sr_2CoRuO_6 were consistent with the adoption of a distorted perovskite structure (Fig. 1) in the monoclinic space group $I2/c$ with unit cell parameters of *ca.* $\sqrt{2}a_p \times \sqrt{2}a_p \times 2a_p$, where a_p is the unit cell parameter of a simple cubic perovskite. In this space group, ordering of two different elements over the octahedral sites is not allowed and the refinements were therefore carried out with a disordered arrangement of Co^{3+} and Ru^{5+} ions on these sites. The same symmetry has been reported previously for the iron analogue Sr_2FeRuO_6 (3). Attempts to refine the crystal structure in other space groups that would permit an ordered arrangement of Co^{3+} and Ru^{5+} were unsuccessful and no evidence was found for a significant concentration of anion vacancies. The refinements of the appropriate atomic parmeters and profile parameters resulted in the agreement factors R_{wp} = 10.0%, R_p = 7.4%, and R_I = 5.4%. The refined values of the structural parameters are given in Table 2. The corresponding bond lengths and bond angles are listed in Table 3 and the observed, calculated, and difference diffraction profiles are shown in Fig. 2.

All the reflections in the powder X ray diffraction data of Ba_2CoRuO_6 could be indexed in a hexagonal unit cell, the size of which was consistent with the 6H-perovskite structure (Fig. 3). The atomic coordinates of $Ba_3NiRu_2O_9$ (7) were used as a starting model for the refinement of the crystal structure, with Ru occupying only the face-sharing octahedra, and only Co occupying the corner-sharing

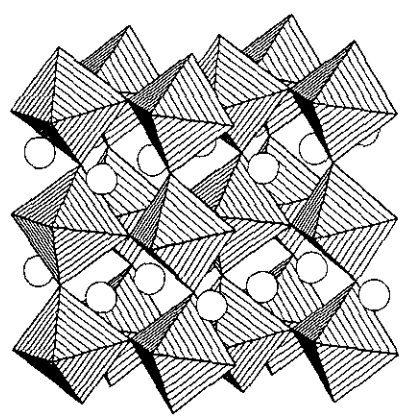

FIG. 1. The distorted, pseudo-cubic perovskite structure showing corner-sharing Co/RuO_6 octahedra; hollow circles represent A and A' cations.

TABLE 2
Structural Parameters for Sr_2CoRuO_6 at Room Temperature

Atom	Site	x	y	z	B_{iso}(Å^2)
Sr	4e	0	0.499(1)	$\frac{1}{4}$	0.18(2)
Co/Ru	4a	0	0	0	0.32(3)
O1	4e	0	0.027(9)	$\frac{1}{4}$	1.21(9)
O2	8f	0.269(4)	0.772(7)	0.017(4)	1.21(9)

Note. a = 5.5279(1), b = 5.5396(1), c = 7.8305(2) Å; β = 90.21(1)°; V = 239.78(1) Å^3

octahedra. Subsequent refinements of the usual atomic parameters and profile parameters in space group $P6_3/mmc$ led to the final agreement factors R_{wp} = 8.6%, R_p = 6.3%, and R_I = 2.4%. No significant concentration of Ru was found in the corner-sharing MO_6 octahedra. The data set was not of sufficient quality to permit refinement of the temperature factors and they were therefore held fixed at 0.0 Å^2. The final atomic coordinates are presented in Table 4 and selected bond lengths and bond angles are listed in Table 5. The observed, calculated, and difference diffraction profiles are plotted in Fig. 4.

(b) $AA'CoRuO_6$ (A = Sr, Ba; A' = La). Powder X ray diffraction data collected on $SrLaCoRuO_6$ indicated that this compound adopts a pseudo-cubic perovskite structure. The presence of a relatively strong reflection at $2\theta \sim 19°$ led us to assume that the Co and Ru cations are ordered over the six-coordinate sites, and the systematic absences in the diffraction pattern were consistent with the monoclinic space group $P2_1/n$. The Sr^{2+} and La^{3+} cations are disordered over one crystallographic site in this space group. Refinements of the usual atomic and profile parameters led to the argeement factors R_{wp} = 10.7%, R_p = 7.6%, and R_I = 4.1%. The Co/Ru distribution over the two crystallographically distinct octahedral sites was allowed to vary, with the constraint that the 1 : 1 ratio was maintained. Individual atomic temperature factors could not be refined and thus the isotropic temperature factors for all the atoms were constrained to be equal. The refined structural parameters, including the fractional occupation number, n, of the Co/Ru site, are listed in Table 6 and bond lengths and bond angles are given in Table 7. The observed, calculated, and difference diffraction profiles are shown in Fig. 5.

$BaLaCoRuO_6$ has been described before (2) as a cubic perovskite, but our data indicate a lower symmetry. Experience gained during studies of the related materials. $BaLaMRuO_6$ (M = Zn, Ni) (3) initially led us to attempt a structure refinement in the monoclinic space group $I2/c$. However, the presence of a reasonably strong reflection at $2\theta \sim 19°$ again suggested that the Co^{2+} and Ru^{5+} ions are ordered over the octahedral B sites and the data were finally analyzed in space group $I2/m$, which can accommodate ordering of the B-site cations. The Ba^{2+} and La^{3+} cations were assumed to be randomly distributed over the A sites. Again, the introduction of partial disorder of Co/Ru over the two crystallographically distinct B sites was necessary to achieve a satisfactory convergence. The isotropic temperature factors of these two sites were constrained to be equal. The X ray diffraction profiles drawn in Fig. 6 derive from the structural parameters of Table 8 and correspond to agreement factors R_{wp} = 9.6%, R_p = 6.9%, and R_I = 1.9%. The most important bond lengths and bond angles are listed in Table 9. Neutron diffraction data collected on $BaLaCoRuO_6$ at room temperature and 1.5 K are shown in Fig. 7. Quantitative analysis of these data proved impossible because of the

TABLE 3
Bond Lengths (Å) and Bond Angles (°) in Sr_2CoRuO_6 at Room Temperature

Co/Ru–O1	1.963(4) × 2	Co/Ru–O2	1.95(2) × 2
Sr–O1		Sr–O2	
2.768(3) × 2		2.97(2) × 2	
2.61(5)		2.80(5) × 2	
2.93(5)		2.76(5) × 2	
		2.56(2) × 2	
O1–Co/Ru–O2	90.7(1)	Co/Ru–O1–Co/Ru	171.3(3)
O1–Co/Ru–O2	90.9(1)	Co/Ru–O2–Co/Ru	168.0(10)
O2–Co/Ru–O2	90.3(2)		

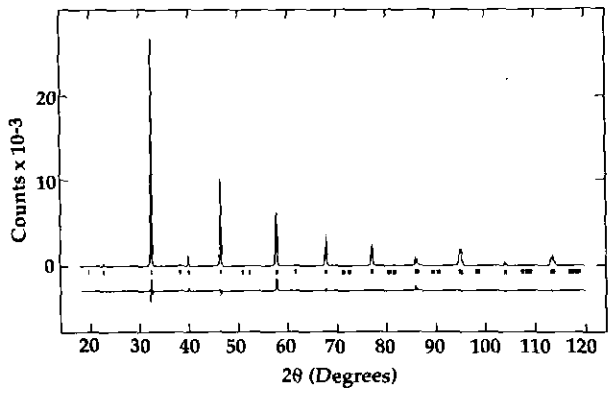

FIG. 2. The observed (points), calculated (solid line), and difference (below) X ray diffraction profiles of Sr_2CoRuO_6. Reflection positions are marked.

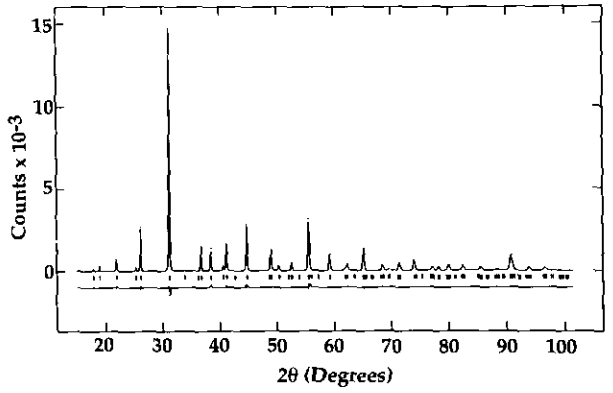

FIG. 4. The observed (points), calculated (solid line), and difference (below) X ray diffraction profiles of Ba_2CoRuO_6. Reflection positions are marked.

combination of a poorly defined peak shape and a high degree of pseudo-symmetry. They are presented here to show qualitatively that no additional (magnetic) Bragg scattering appears in the diffraction pattern as a result of phase changes occuring between room temperature and 1.5 K.

(ii) Electrical Measurements

The resistivities of the compounds under discussion are plotted as a function of temperature in Fig. 8. All the samples are semiconducting in the range $77 \leq T \leq 300$ K. Attempts to fit the observed data to a simple Arrhenius model were unsuccessful, as were those based on a small-polaron mechanism. Taking into account the Mott variable-range hopping (VRH) behavior found in many perovskite-related materials (*11–13*), a least-squares fit of the data to the equation

$$\rho = \rho_0(T/T_0)^{1/2} \exp((T_0/T)^{\nu})$$

was carried out. Excellent agreement was obtained between experiment and theory but, owing to the limited temperature range over which the data were collected, the level of agreement was insensitive to the exponent, ν, and consequently to the dimensionality of the hopping process. The results of the linear fits for $\ln(\rho T^{-1/2})$ versus $T^{-1/4}$ (3D hopping) are plotted in Fig. 9, but the agreement is not significantly worse if a 2D mechanism ($\nu = 1/3$) is assumed.

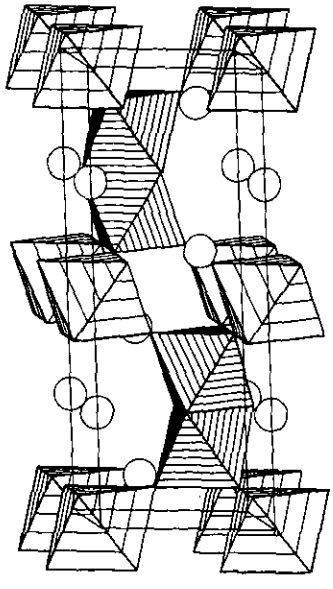

FIG. 3. The 6H-hexagonal perovskite structure with corner-sharing and face-sharing Co/RuO_6 octahedra; hollow circles represent A and A' cations.

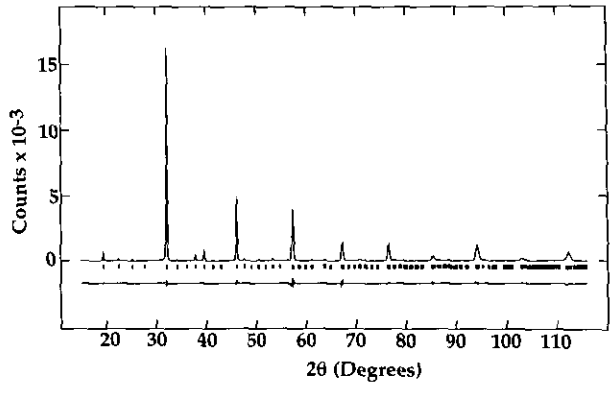

FIG. 5. The observed (points), calculated (solid line), and difference (below) X ray diffraction profiles of $SrLaCoRuO_6$. Reflection positions are marked.

TABLE 4
Structural Parameters for Ba_2CoRuO_6 at Room Temperature

Atom	Site	x	y	z	n
Ba1	2b	0	0	$\frac{1}{4}$	
Ba2	4f	$\frac{1}{3}$	$\frac{2}{3}$	0.91025(7)	
Co1	4f	$\frac{1}{3}$	$\frac{2}{3}$	0.15483(9)	0.25
Ru1	4f	$\frac{1}{3}$	$\frac{2}{3}$	0.15483(9)	0.75
Co2	2a	0	0	0	
O1	6h	0.4902(7)	−0.020(1)	$\frac{1}{4}$	
O2	12k	0.1642(6)	0.328(1)	0.4142(3)	

Note. a = 5.72646(9), c = 14.0593(3) Å; V = 399.27(2) Å^3; B_{iso} = 0.0 Å^2. n is the fractional site occupancy (=1 unless stated).

TABLE 5
Bond Lengths (Å) and Bond Angles (°) in Ba_2CoRuO_6 at Room Temperature

Co/Ru1–O1	2.052(5) × 3	Co2–O2	2.026(5) × 6
Co/Ru1–O2	1.939(5) × 3	Co/Ru1–Co2	2.676(3)
Ba1–O1	2.865(1) × 6	Ba2–O2	2.864(1) × 6
Ba1–O2	2.825(5) × 6	Ba2–O2′	2.984(5) × 3
Ba2–O1	2.853(4) × 3		
O1–Co/Ru1–O1	82.1(2)	O2–Co2–O2	88.2(2)
O1–Co/Ru1–O2	89.9(2)	Co2–O2–Co/Ru1	173.5(3)
O2–Co/Ru1–O1	169.4(2)		

TABLE 6
Structural Parameters for $SrLaCoRuO_6$ at Room Temperature

Atom	Site	x	y	z	n
Sr/La	4e	−0.0026(6)	0.0206(1)	0.2554(3)	
Co1	2d	$\frac{1}{2}$	0	$\frac{1}{2}$	0.894(6)
Ru1	2d	$\frac{1}{2}$	0	$\frac{1}{2}$	0.106(6)
Co2	2c	$\frac{1}{2}$	0	0	0.106(6)
Ru2	2c	$\frac{1}{2}$	0	0	0.894(6)
O1	4e	0.268(3)	0.263(3)	0.040(2)	
O2	4e	0.225(4)	−0.206(4)	0.029(3)	
O3	4e	−0.070(3)	0.493(1)	0.263(2)	

Note. a = 5.5693(3), b = 5.5679(3), c = 7.8858(3) Å; β = 90.28(1)°; V = 244.53(2) Å^3; B_{iso} = 0.06(2) Å^2.

TABLE 7
Bond Lengths (Å) and Bond Angles (°) in $SrLaCoRuO_6$ at Room Temperature

Co/Ru1–O1	2.02(2) × 2	Co/Ru2–O1	1.98(2) × 2
Co/Ru1–O2	2.07(2) × 2	Co/Ru2–O2	1.93(2) × 2
Co/Ru1–O3	2.11(2) × 2	Co/Ru2–O3	1.91(2) × 2

Sr/La–O1	Sr/La–O2	Sr/La–O3
3.18(2)	3.17(2)	2.063(8)
2.64(2)	2.75(3)	2.39(2)
2.52(2)	2.53(2)	2.657(8)
2.86(2)	2.76(2)	3.20(2)

O1–Co/Ru1–O2	93.1(11)	O1–Co/Ru2–O2	95.7(11)
O1–Co/Ru1–O3	91.6(8)	O1–Co/Ru2–O3	90.7(8)
O2–Co/Ru1–O3	91.2(7)	O2–Co/Ru2–O3	91.7(8)

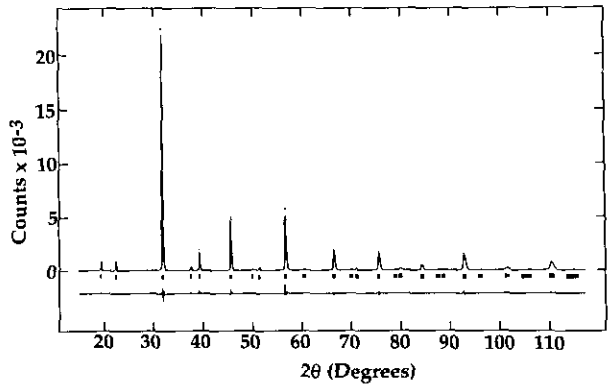

FIG. 6. The observed (points), calculated (solid line), and difference (below) X ray diffraction profiles of $BaLaCoRuO_6$. Reflection positions are marked.

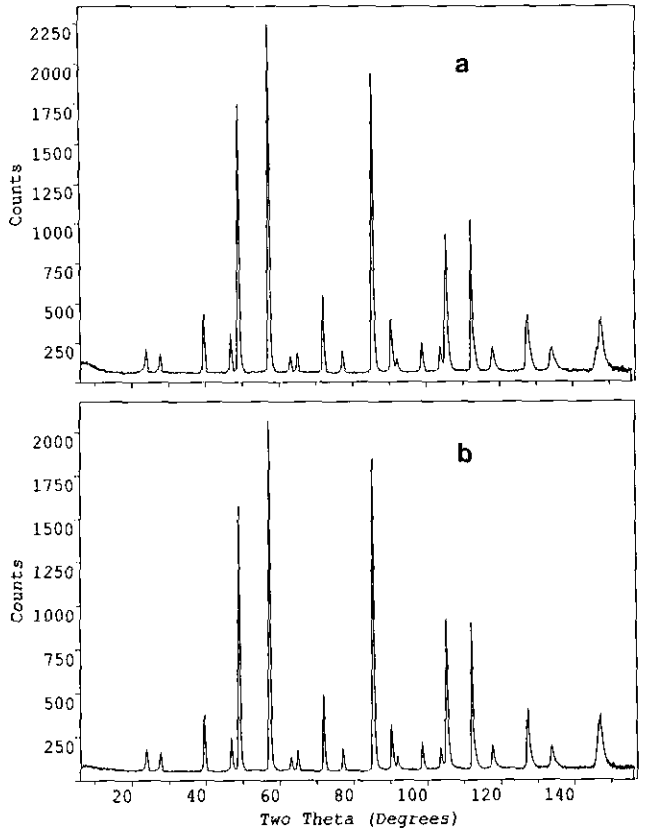

FIG. 7. The neutron powder diffraction profiles of $BaLaCoRuO_6$ at (a) 1.5 K and (b) room temperature.

(iii) Magnetic Measurements

The molar magnetic susceptibility of Sr_2CoRuO_6, measured in applied fields of 1 and 5 kG, is plotted as a function of temperature in Fig. 10. Both the ZFC and FC data reach a maximum at *ca.* 95 K. Taken alone, this behavior might be considered to indicate the onset of long-range antiferromagnetic order. However, the divergence of the two curves at low temperatures suggests that this compound is not a classical Néel antiferromagnet, but rather that its magnetic properties are frustrated in nature. Furthermore, the magnitude of the FC susceptibility is dependent on the strength of the applied field. The ZFC and FC curves measured in 5 kG overlie each other down to 95 K. When the applied field is decreased to 1 kG, however, the FC curve begins to diverge significantly from the ZFC curve at *ca.* 250 K. Analysis, using the Curie–Weiss Law, of the limited data available at $T >$ 250 K leads to the values $\theta = -70$ *K*, $\mu_{eff} = 2.99\ \mu_B$ per magnetic ion.

The ZFC and FC susceptibilities of Ba_2CoRuO_6 are plotted as a function of temperature in Fig. 11. At high temperatures (above *ca.* 200 K) the FC and ZFC data overlie each other quite closely and obey a Curie–Weiss Law with $\theta = -26$ K and $\mu_{eff} = 3.20\ \mu_B$ per magnetic ion. Nonetheless, magnetic irreversibility is again apparent at low temperatures; while the ZFC data show a broad susceptibility maximum at *ca.* 35 K, the FC curve continues to increase below this point. A field dependence of the FC data was again observed at low temperatures ($T <$

TABLE 8
Structural Parameters for $BaLaCoRuO_6$ at Room Temperature

Atom	Site	*x*	*y*	*z*	B_{iso}(Å^2)	*n*
Ba/La	4i	0.5033(4)	0	0.2484(3)	0.48(2)	
Co1	2a	0	0	0	0.17(2)	0.906(7)
Ru1	2a	0	0	0	0.17(2)	0.094(7)
Co2	2c	0	0	$\frac{1}{2}$	0.17(2)	0.094(7)
Ru2	2c	0	0	$\frac{1}{2}$	0.17(2)	0.906(7)
O1	4i	0.045(3)	0	0.265(3)	0.4(2)	
O2	8j	0.235(2)	0.271(2)	0.027(2)	0.4(2)	

Note. $a = 5.6266(2)$, $b = 5.6416(2)$, $c = 7.9856(2)$ Å; $\beta = 90.12(1)°$; $V = 253.48(1)$ Å^3.

TABLE 9
Bond Lengths (Å) and Bond Angles (°) in $BaLaCoRuO_6$ at Room Temperature

Co/Ru1–O1	2.13(2) × 2	Co/Ru2–O1	1.89(2) × 2
Co/Ru1–O2	2.03(1) × 4	Co/Ru2–O2	1.99(1) × 4
Ba/La–O1		Ba/La–O2	
2.836(2) × 2		3.06(1) × 2	
2.58(2)		2.88(2) × 2	
3.05(2)		2.78(2) × 2	
		2.59(1) × 2	
O1–Co/Ru1–O2	100.4(4)	O1–Co/Ru2–O2	102.1(5)
O2–Co/Ru1–O2	97.6(8)	O2–Co/Ru2–O2	98.8(8)
		Co/Ru1–O2–Co/Ru2	165.2(7)

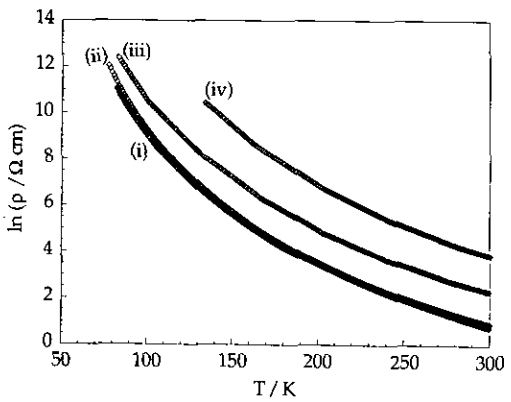

FIG. 8. The resistivity of mixed Co/Ru perovskites as a function of temperature: (i) Sr_2CoRuO_6, (ii) Ba_2CoRuO_6, (iii) $SrLaCoRuO_6$, and (iv) $BaLaCoRuO_6$.

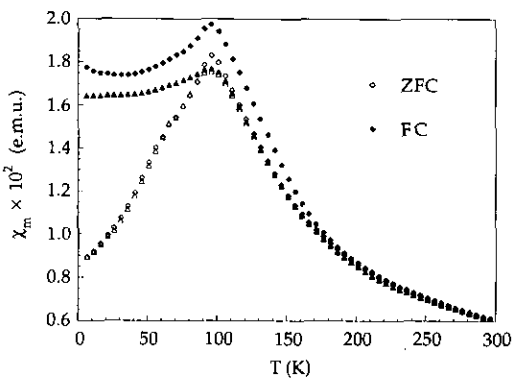

FIG. 10. The temperature dependence of the ZFC (hollow symbols) and FC (filled symbols) molar magnetic susceptibility of Sr_2CoRuO_6. Fields of 1 (diamond) and 5 kG (triangle) were applied.

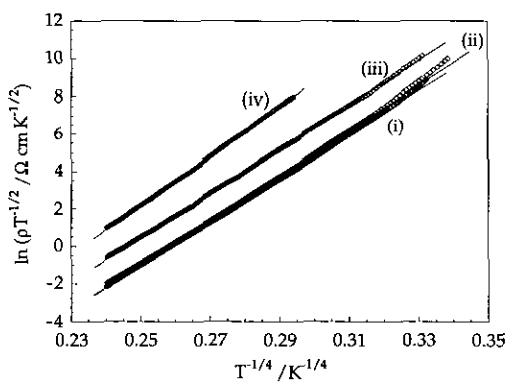

FIG. 9. ln $(\rho T^{-1/2})$ versus $T^{-1/4}$ for (i) Sr_2CoRuO_6, (ii) Ba_2CoRuO_6, (iii) $SrLaCoRuO_6$, and (iv) $BaLaCoRuO_6$.

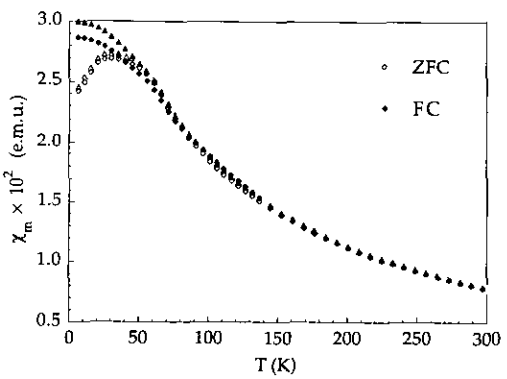

FIG. 11. The temperature dependence of the ZFC (hollow symbols) and FC (filled symbols) molar magnetic susceptibility of Ba_2CoRuO_6. Fields of 1 (diamond) and 5 kG (triangle) were applied.

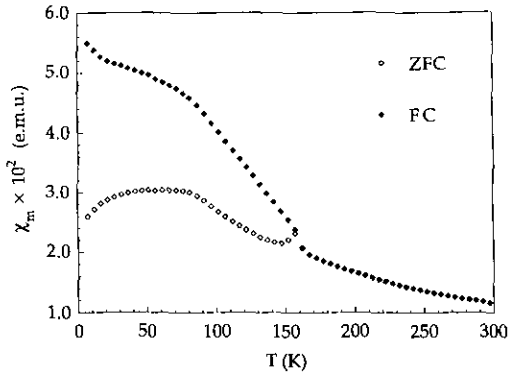

FIG. 12. The ZFC (hollow symbols) and FC (filled symbols) molar magnetic susceptibility of $SrLaCoRuO_6$ as a function of temperature, collected in an applied field of 1 kG.

70 K), although, in contrast to the behavior of Sr_2CoRuO_6 described above, the magnitude of the FC susceptibility is increased rather than reduced as the applied field increases.

Figure 12 shows that the partially ordered perovskite $SrLaCoRuO_6$ exhibits more complex magnetic behavior. The ZFC data show a sharp cusp at *ca.* 157 K, and below this temperature the two curves show very different temperature dependencies; the FC susceptibility continues to rise as the temperature decreases, whereas anomalous behavior is observed in the ZFC data. Both the ZFC and FC curves display a change of slope at *ca.* 30 and *ca.* 80 K. This, together with the observation of the magnetic irreversibility, indicates that complex magnetic interactions are occurring at low temperatures in this sample. The FC susceptibility overlays the ZFC curve above 157 K. The data at $T > 200$ K can be well fitted to a Curie–Weiss law with $\theta = -22$ K, $\mu_{eff} = 3.67\ \mu_B$ per magnetic cation.

The temperature variation of the molar susceptibility of $BaLaCoRuO_6$ is plotted in Fig. 13. The ZFC and FC curves agree well down to *ca.* 40 K at which temperature the ZFC data exhibit a maximum. The FC curve also has a maximum at *ca.* 40 K, but a divergence of the ZFC and FC data is apparent below this point. Figure 13 also shows a nonlinear field dependence of the FC magnetisation at $T < 40$ K. Analysis of the data at $T > 200$ K leads to a Weiss constant of +34 K and a molar Curie constant of 4.02 emu/mol K. The latter corresponds to the effective magnetic moment of 4.01 μ_b per magnetic ion. The observation of the small, positive Weiss constant and the transition temperature of *ca.* 40 K is consistent with the results of Fernandez *et al.* (2).

The magnetic behavior of $Ba_3CoRu_2O_9$ differs markedly from that of the compounds described above. The molar magnetic susceptibilities of $Ba_3CoRu_2O_9$, measured in an applied field of 1 kG, are shown in Fig. 14. The ZFC and FC curves overlay each other over the measured temperature range and both of the curves show maximum at *ca.* 106 K, indicating that below this temperature the sample is antiferromagnetic, in agreement with the results of our previous neutron diffraction studies (7), Fitting of the high temperature data ($T > 200$ K) to a Curie–Weiss law leads to the following values of the effective magnetic moment and Weiss constant: $\mu_{eff} = 4.06\ \mu_B$ per magnetic ion and $\theta = -190$ K.

DISCUSSION

As expected, all of our target compounds adopt perovskite-related crystal structures; Ba_2CoRuO_6 has a 6H hexagonal structure and the remaining compounds all adopt a pseudo-cubic form. This is consistent with the well-established rule that the tendency of the AO_3 pseudo-close-packed layers within the structure to pack in a hexagonal manner increases with the ratio of the cation sizes, r_A/r_B. The consequence of this structural difference is that $Ba_2Co\ RuO_6$ contains face-sharing octa-

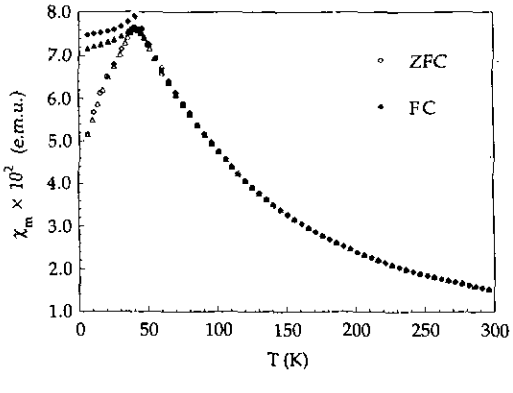

FIG. 13. The temperature dependence of the ZFC (hollow symbols) and FC (filled symbols) molar magnetic susceptibility of $BaLaCoRuO_6$. Fields of 1 (diamond) and 5 kG (triangle) were applied.

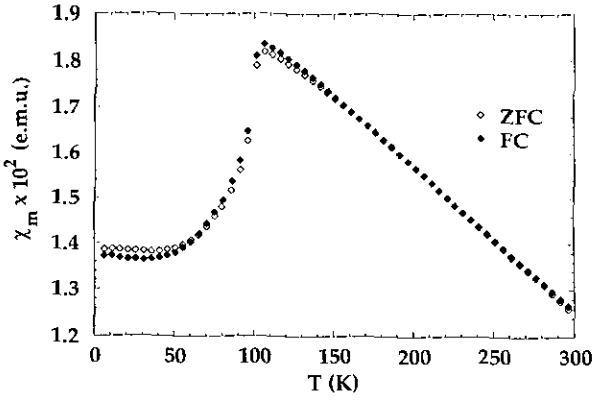

FIG. 14. The ZFC (hollow symbols) and FC (filled symbols) molar magnetic susceptibility of $Ba_3CoRu_2O_9$ as a function of temperature, collected in an applied field of 1 kG.

hedra in addition to the cornersharing polyhedra found in the pseudo-cubic from (Fig. 1 and 3). None of the structures described for the first time above contains a fully ordered distribution of Ru and Co cations. In the case of Ba_2CoRuO_6, the cornersharing octahedra contain Co only, but there is a random distribution of Ru and Co (albeit in a 3 : 1 ratio) over the face-sharing sites. The two transition metal cations are distributed randomly over the six-coordinate sites in Sr_2CoRuO_6 and in a partially (~90%) ordered way in both $SrLaCoRuO_6$ and $BaLaCoRuO_6$. This can be contrasted with the other compound discussed above, $Ba_3CoRu_2O_9$, which has a 6H structure with the face-sharing sites occupied only by Ru and the corner-sharing site occupied only by Co. We will refer to the extent of the cation disorder again when discussing the magnetic properties of these compounds. In that discussion it will be necessary to make assumptions about the oxidation states of the Co and Ru cations. Our electrical data suggest that it is reasonable to discuss the properties of these materials in terms of a localized electron model and there is little doubt that in the cases of Ba_2CoRuO_6 and Sr_2CoRuO_6 we are dealing with Co^{3+} and Ru^{5+}. Mössbauer measurements on $BaLaCoRuO_6$ and $Ba_3CoRu_2O_9$ (2, 14) characterized the Ru in these compounds as being pentavalent and we will therefore assume that $SrLaCoRuO_6$ also contains Co^{2+} and Ru^{5+} rather than Co^{3+} and Ru^{4+}. In perovskite-related materials, for example, the brownmillerite Sr_2CoO_5 (15), Co^{3+} occurs in a high-spin state, rather than the diamagnetic low-spin form, and we will assume that Ba_2CoRuO_6 and Sr_2CoRuO_6 also contain high-spin Co^{3+}. The average cation magnetic moments reported above are too large to be due to Ru only, and it would be most surprising if Ru^{5+} alone could lead to the observation of a susceptibility maximum at 95 K in Sr_2CoRuO_6 when other compounds containing only this magnetic species have $T_N < 40$ K (1, 2, 4). Furthermore, the bond lengths listed in Tables 3 and 5 are consistent with the presence of high-spin Co^{3+}, although we would not want to claim too high an accuracy for these values, given that they were deduced from an X ray powder diffraction experiment. However, all the structural data we have presented above are compatible with our assumptions and the discussion that follows.

In considering the magnetic properties of these Co/Ru compounds, it is convenient to begin with $Ba_3CoRu_2O_9$. The data in Fig. 14 show that this compound orders antiferromagnetically at 106 K, and there is no evidence for the presence of magnetic frustration. It has been shown (16) that the cations in Ru_2O_9 dimers formed by face-sharing RuO_6 octahedra undergo spin pairing at temperatures of ~300 K, and the transition at 106 K is therefore likely to correspond to the onset of the long-range magnetic ordering, involving the Co^{2+} ions, that was characterized in our earlier neutron diffraction study (7). The point to be emphasized here is that in a structurally ordered Co/Ru oxide, antiferromagnetism occurs without any frustration. The susceptibility data collected from $Ba_3CoRu_2O_9$ can be contrasted with those from another 6H perovskite, Ba_2CoRuO_6 (or $Ba_3Co_{3/2}Ru_{3/2}O_9$) which are shown in Fig. 11. The latter show a maximum at ~35 K rather than 106 K, and the ZFC and FC susceptibilities diverge below this point. The nature of the superexchange interactions (antiferromagnetic, ferromagnetic) between the cation sites in corner-sharing octahedra is not likely to change on moving from $Co^{2+}: 3d^7$ to $Co^{3+}: 3d^6$ and we therefore ascribe the change in magnetic behavior to the presence of cation disorder in the M_2O_9 dimers. Some of these units will still contain pairs of Ru cations, but others will contain Co/Ru pairs. The range of superexchange interactions created by this structural disorder is apparently great enough to prevent the formation of an antiferromagnetic state and to give rise to what appears to be a spin-glass transition at 35 K. However, neutron diffraction data are needed to demonstrate unambiguously the absence of long-range magnetic order in the low-temperature phase of this compound. Such data are available (Fig. 7) for the pseudo-cubic perovskite $BaLaCoRuO_6$ and they show no evidence of magnetic ordering. This compound has a partially ordered arrangement of $Ru^{5+}: 4d^3$ and $Co^{2+}: 3d^7$ ions over the vertex-sharing, six-coordinate sites and the hysteresis in the magnetic susceptibility data (Fig. 13) again suggests a low-temperature transition to a spin-glass state. The temperature at which this transition occurs, ~40 K, is similar to that recorded in the case of a related spin-glass compound, $BaLaNiRuO_6$ (3). A wide range of superexchange interactions are present in $BaLaCoRuO_6$. We can assume that the interaction between Co/Co and Ru/Ru pairs on nearest-neighbor (NN) sites is always antiferromagnetic, but, because of the nature of the coupling between a d^7 ion and a d^3 ion (17), the Co/Ru interaction is expected to be ferromagnetic if the Co–O–Ru superexchange pathway is close to linear. Our X ray powder diffraction data show (Table 9) that the angle at the oxide ion is ~165° in $BaLaCoRuO_6$, a departure from linearity which may well be large enough to lead to antiferromagnetic Co/Ru coupling, although the positive value of the Weiss temperature, θ, suggests that some ferromagnetic interactions are present. Whatever the sign of the Co/Ru interaction, the cation sublattice in $BaLaCoRuO_6$ is not prone to magnetic frustration and the formation of a magnetically ordered ground state would normally be expected; the occurrence of a spin-glass phase cannot be explained in terms of NN interactions alone. However, the magnetic structures adopted by other Ru oxides (1) demonstrate that the interactions between next-nearest-neighbor (NNN) cations in $BaLaCoRuO_6$ are not insignificant, and we believe that magnetic

frustration apparent in this compound arises through the competition between NN and NNN interactions. Similar arguments have been put forward to explain the behavior of other perovskite spin glasses, for example, Sr_2FeNbO_6 (18).

The magnetic behavior of the two strontium compounds described in this study is also complex, with hysteresis effects becoming apparent at temperatures that are relatively high compared to those seen in the barium analogues. This reflects in part the sensitivity of the magnetic exchange constants to interatomic distance. The magnetic susceptibility of Sr_2CoRuO_6 bears some resemblance to that of $SrLaCuRuO_6$, another pseudo-cubic perovskite with a disordered distribution of transition metal cations (5). The hysteresis observed between 100 and 200 K in the data collected in a field of 1 kG can be ascribed to the presence of blocked spin clusters, each of which carries a net magnetic moment; the application of a higher field limits the growth of the clusters in such a way that blocking does not occur. By analogy with $SrLaCuRuO_6$, the susceptibility maximum at ~100 K could correspond to a transition to a spin-glass state, although the corresponding transition occurs at the much lower temperature of 22 K in the Cu compound; Sr_2FeRuO_6 (3), which has a closer structural relationship to Sr_2CoRuO_6, has $T_g \sim 50$ K. Confirmation by neutron diffraction of the absence of long-range magnetic order in the Co analogue would be particularly desirable in view of the unusually high freezing temperature. The magnetic properties of $SrLaCoRuO_6$ are more difficult to interpret from the data presently available. The transition temperature (~155 K) is significantly higher than that seen in Sr_2CoRuO_6, whereas the Co^{3+} ($S = 2$) compound would normally be expected to show the stronger magnetic interactions. Furthermore, the temperature dependence of the magnetic susceptibility of $SrLaCoRuO_6$ is very different to that shown by all the other compounds in this study and suggests that the extensive cation ordering in this compound leads to the formation of a low-temperature phase which has a backbone of magnetically ordered spins, but also that the residual disorder causes a number of frustrated spins to remain decoupled, thus introducing hysteresis into the data. Similar behavior has been observed in disordered $SrLaFeSnO_6$ (19). The exchange interactions in $BaLaCoRuO_6$, which shows a similar degree of cation ordering to $SrLaCoRuO_6$, are weakened by the relative increase in the interatomic distances and only spin-glass ordering occurs in the former compound. A neutron diffraction study is needed to test this model for the behavior of $SrLaCoRuO_6$.

In conclusion, we have shown that complex magnetic behavior can result when two alioelectronic cations are distributed in a disordered manner over the sites of a nonfrustrated lattice. Susceptibility data consistent with spin-glass behavior are seen in such cases, for example, $BaLaCoRuO_6$. Long-range antiferromagnetic order occurs when the same two cations adopt a structurally ordered array, for example, in $Ba_3CoRu_2O_9$.

ACKNOWLEDGMENTS

We are grateful to the SERC for financial support. S.H.K. was funded by an ICI Scholarship.

REFERENCES

1. P. D. Battle and W. J. Macklin, *J. Solid State Chem.* **52,** 138 (1984).
2. I. Fernandez, R. Greatrex, and N. N. Greenwood, *J. Solid State Chem.* **32,** 97 (1980).
3. P. D. Battle, T. C. Gibb, C. W. Jones, and F. Studer, *J. Solid State Chem.* **78,** 281 (1989).
4. P. D. Battle, C. W. Jones, and F. Studer, *J. Solid State Chem.* **90,** 302 (1991).
5. S. H. Kim and P. D. Battle, *J. Magn. Magn. Mater.* **123,** 273 (1993).
6. P. D. Battle, S. K. Bollen, and A. V. Powell, *J. Solid State Chem.* **99,** 267 (1992).
7. P. Lightfoot and P. D. Battle, *J. Solid State Chem.* **89,** 174 (1990).
8. H. M. Rietveld, *J. Appl. Crystallogr.* **2,** 65 (1969).
9. A. C. Larson and R. B. Von Dreele, "General Structure Analysis System (GSAS)." Los Alamos National Laboratory Report, LAUR 86-748, 1990.
10. C. J. Howard, *J. Appl. Crystallogr.* **15,** 615 (1982).
11. M. A. Kastner, R. J. Birgeneau, C. Y. Chen, Y. M. Chiang, D. R. Gabbe, H. P. Jenssen, T. Junk, C. J. Peters, P. J. Picone, Tineke Thio, T. R. Thurston, and H. L. Tuller, *Phys. Rev. B* **37,** 111 (1988).
12. M. J. Rosseinsky, K. Prassides, and P. Day, *J. Mater. Chem.* **1,** 597 (1991).
13. T. J. Goodwin, H. B. Radousky, and R. N. Shelton, *Physica, C* **204,** 212 (1992).
14. I. Fernandez, R. Greatrex, and N. N. Greenwood, *J. Solid State Chem.*, **34,** 121 (1980).
15. T. Takeda, Y. Yamaguchi, and H. Watanabe, *J. Phys. Soc. Jpn.* **33,** 970 (1972).
16. J. Darriet, M. Drillon, G. Villeneuve, and P. Hagenmuller, *J. Solid State Chem.* **19,** 213 (1976).
17. J. B. Goodenough, "*Magnetism and the Chemical Bond.*" Wiley, New York, 1963.
18. R. Rodriguez, A. Fernandez, A. Isalgue, J. Rodriguez, A. Labarta, J. Tejada, and X. Obradors, *J. Phys. C: Solid State Phys.* **18,** L401 (1985).
19. M. P. Attfield, P. D. Battle, S. K. Bollen, T. C. Gibb, and R. J. Whitehead, *J. Solid State Chem.* **100,** 37 (1992).